Dilepton Radiation from Cascading Partons in Ultrarelativistic Nuclear Collisions

K. Geiger and J. I. Kapusta

School of Physics and Astronomy, University of Minnesota, Minneapolis, Minnesota 55455

We compute the radiation of lepton pairs by the quarks during a central collision between gold nuclei at energy of the Brookhaven Relativistic Heavy Ion Collider ($\sqrt{s} = 200A$ GeV) within the parton cascade model. The distribution of radiated pairs evolves smoothly from the initial Drell-Yan type reactions all the way towards equilibrium radiation. Contributions from reactions involving secondary partons dominate the Drell-Yan yield by at least a factor of 5 even at an invariant mass of 8 GeV. Therefore, experiments can test the evolution of partons towards thermal equilibrium at these energies.

PACS numbers: 25.75.+r, 12.38.Mh, 24.85.+p

The possibility of producing a dense plasma of quarks and gluons in a central collision between two massive nuclei may be realized in the near future at the Relativistic Heavy Ion Collider (RHIC) under construction at Brookhaven National Laboratory. How to gather information on this new phase of matter has been a long-standing problem. One early suggestion [1] was to calculate and measure the yield of lepton pairs radiated by quarks and antiquarks as they are created, annihilated, and scattered. The leptons are produced mainly when the energy density is a maximum; they escape from the system unscathed to carry information about the high density matter to the detectors. Usually one calculates the Drell-Yan contribution and considers it a background to the yield from a thermalized quark-gluon plasma, the temperature of the latter decreasing with time because of hydrodynamic expansion [2]. However, this is an unsatisfactory state of affairs, because there is an uncertainty in choosing the formation time and temperature of the plasma. One would really like to have a dynamical calculation that would evolve the initial partons smoothly from their first hard scattering, through a preequilibrium stage, and into a fully thermalized plasma. This is now possible with the parton cascade model [3–5]. In this Letter we report on the calculation of the yield of lepton pairs within the parton cascade.

Conceptually, the production of dileptons is ideal for probing the dynamics of the charged particles (quarks and antiquarks), because the coupling of (virtual) photons to quarks is the same as the coupling of gluons to quarks except for the strength of the coupling constant and a color matrix. We take into account the following elementary processes, in which a pair of colliding partons (quarks q, antiquarks $\bar{q}$, or gluons g) directly produces a timelike photon that subsequently decays into an l^+l^- pair (l is an electron or muon),

$$q + \bar{q} \to \gamma^* \to l^+ + l^- , \tag{1}$$
$$q + \bar{q} \to \gamma^* + g \to l^+ + l^- + g , \tag{2}$$
$$g + q(\bar{q}) \to \gamma^* + q(\bar{q}) \to l^+ + l^- + q(\bar{q}), \tag{3}$$
$$g + g \to \gamma^* + g \to l^+ + l^- + g , \tag{4}$$

plus the bremsstrahlung processes in which a timelike virtual quark or antiquark radiates a photon that subsequently yields a l^+l^- pair,

$$q(\bar{q}) \to \gamma^* + q(\bar{q}) \to l^+ + l^- + q(\bar{q}) . \tag{5}$$

Figure 1(a) depicts these processes in terms of Feynman diagrams. Recall that in the parton cascade model the complicated space-time structure of multiple parton interactions is pictured as many internetted cascades composed of elementary $2 \to 2$ collisions, $2 \to 1$ fusion processes, and $1 \to 2$ branchings, plus higher order virtual and real corrections [3, 4]. Therefore, the subset of pro-
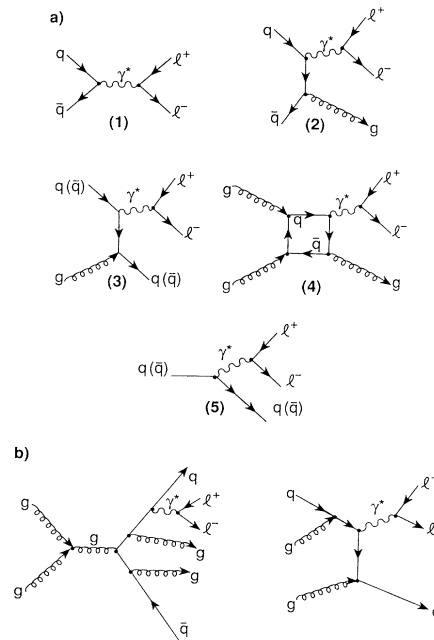

FIG. 1. (a) Feynman diagrams for the lowest order QCD processes to produce an l^+l^- pair through parton-parton collisions (1)–(4), or through bremsstrahlung by a virtual quark or antiquark (5). (b) Examples of higher order processes that are effectively accounted for in the present approach by decomposing them into the elementary processes (1)–(5).

cesses (1)–(5) is much more general than it seems at first sight. For example, as illustrated in Fig. 1(b), the higher order process $g + g \rightarrow q + \bar{q} + 2g + l^+ + l^-$ is included in the form of two gluon annihilation into a $q\bar{q}$ pair where the q and the $\bar{q}$ both emit a gluon, and the quark in addition radiates a γ^* that yields a l^+l^- pair. Similarly, processes with three or more partons in the initial state are also accounted for. For instance, the process $q + g + g \rightarrow q + g + l^+ + l^-$ is decomposed into the absorption of a gluon by the incoming quark, the collision of the quark with another gluon, and the radiative photon emission by the outgoing quark where the photon decays into a lepton pair.

The space-time history of dilepton production in a nuclear collision is extracted from the time development of the phase-space distributions $F_a(p, r)$ for the partons of species $a = q_f, \bar{q}_f, g$ (f labeling the quark flavors), starting from their given initial form at time $t = t_0$ when the two nuclei begin to overlap. The time evolution is governed by a relativistic transport equation with Lorentz invariant collision integrals that involve the matrix elements for the different kind of interaction processes in which at least one parton of type a is involved. Its specific form is given in Ref. [4].

In the following we are concerned only with the subset of processes (1)–(5) in which an interaction of a parton of species a results in the production of a lepton pair. Thus, we are interested in the dilepton rates

$$R_{a;\,l^+l^-}(r) = \sum_{b,X} r^{(1)}_{ab \rightarrow l^+l^- X}(r) + \sum_Y r^{(2)}_{a \rightarrow l^+l^- Y}(r), \tag{6}$$

with either two partons or one parton in the initial state and generally $X = (x_1, \ldots, x_m)$, respectively, $Y = (y_1, \ldots, y_n)$, in the final state in addition to a l^+l^- pair. In our case, we have for the process (1) $m = 0$, for (2)–(4) $m = 1$ with $X = q, \bar{q}$, or g, and for (5) $n = 1$ with $Y = q$ or $\bar{q}$. The contributions $r^{(1)}$ and $r^{(2)}$ are given in terms of phase-space integrals involving the matrix elements for the various processes,

$$r^{(1)}_{ab \rightarrow l^+l^- X}(r) = S_{ab} \prod_{j=1}^m \int \frac{d^3 p_j}{(2\pi)^3 2E_j} F_a(1) F_b(2) \left[1 - F_{l^+}(3)\right]\left[1 - F_{l^-}(4)\right]$$

$$\times \prod_{k=5}^m \left[1 + \theta_{x_k} F_{x_k}(k)\right] (2\pi)^4 \delta^4\left(p_1 + p_2 - p_3 - p_4 - \sum_{k=5}^m p_k\right) |M_{ab \rightarrow l^+l^- X}|^2, \tag{7}$$

$$r^{(2)}_{a \rightarrow l^+l^- Y}(r) = \prod_{j=1}^m \int \frac{d^3 p_j}{(2\pi)^3 2E_j} F_a(1) \left[1 - F_{l^+}(3)\right]\left[1 - F_{l^-}(4)\right]$$

$$\times \prod_{k=4}^m \left[1 + \theta_{y_k} F_{y_k}(k)\right] (2\pi)^4 \delta^4\left(p_1 - p_3 - p_4 - \sum_{k=4}^m p_k\right) |M_{a \rightarrow l^+l^- Y}|^2. \tag{8}$$

The spin and color averaged squared matrix elements are weighted by F_α for the incoming particles and $[1 + \theta_\alpha F_\alpha]$ for the outgoing particles, where $\theta_\alpha = -1$ for fermions and $\theta_\alpha = +1$ for bosons. The factor $S_{ab} = (1 + \delta_{ab})^{-1}$ in (8) takes into account the indistinguishability of two identical particles in the initial state [it only affects process (4)].

The total number of dileptons emitted per unit space-time is given by summing (6) over all parton flavors a that contribute to the processes (1)–(5). Using $d^4 r = \tau \, d\tau \, d\eta \, d^2 r_\perp$, where τ is the proper time, η the space-time rapidity, and $r_\perp$ the transverse coordinate, we arrive at the experimentally observable, space-time integrated number distribution of produced l^+l^- pairs with invariant mass squared M^2:

$$\frac{dN}{dM^2} = \int \tau \, d\tau \, d\eta \, d^2 r_\perp \left\{ \sum_{a,b,X} \int_0^\infty d\hat{s} \left(\frac{d\hat{\sigma}_{ab \rightarrow l^+l^- X}/dM^2}{\sum_{c,d} \hat{\sigma}_{ab \rightarrow cd}}\right) \left(\sum_{c,d} \frac{dn_{ab \rightarrow cd}}{d\hat{s}}(\hat{s}; r)\right)\right.$$

$$\left. + \sum_{a,Y} \int_0^\infty dq_a^2 \left(\frac{d\hat{\Gamma}_{a \rightarrow l^+l^- Y}/dM^2}{\sum_{c,d} \hat{\Gamma}_{a \rightarrow cd}}\right) \left(\sum_{c,d} \frac{dn_{a \rightarrow cd}}{dq_a^2}(q_a^2; r)\right)\right\}. \tag{9}$$

Here the dilepton production cross sections $\hat{\sigma}$ for $ab \rightarrow l^+l^- X$ and widths $\hat{\Gamma}$ for $a \rightarrow l^+l^- Y$ are given in terms of the squared amplitudes for the production of a virtual photon of mass M,

$$\frac{d\hat{\sigma}_{ab \rightarrow l^+l^- X}}{dM^2} = \frac{\alpha}{48\pi^2 \hat{s}^2 M^2} \int_{\hat{t}_{\min}}^{\hat{t}_{\max}} d\hat{t} \, F_a \, F_b \, [1 - F_{l^+}]\,[1 - F_{l^-}]$$

$$\times \prod_{k=5}^m \left[1 + \theta_{x_k} F_{x_k}\right] (2\pi)^4 \delta^4\left(\hat{s} + \hat{t} + \hat{u} - M^2 - \sum_{k=5}^m m_{x_k}^2\right) |M_{ab \rightarrow \gamma^* X}(\hat{s}, \hat{t}, M_{\gamma^*}^2)|^2, \tag{10}$$

$$\frac{d\hat{\Gamma}_{a \rightarrow l^+l^- Y}}{dM^2} = \frac{\alpha}{6\pi q_a M^2} \int_{q_{\min}^2}^{q_{\max}^2} dq^2 \, F_a \, [1 - F_{l^+}]\,[1 - F_{l^-}]$$

$$\times \prod_{k=4}^n \left[1 + \theta_{y_k} F_{y_k}\right] (2\pi)^4 \delta^4\left(q_a^2 - M^2 - \sum_{k=4}^n q_{y_k}^2\right) |M_{a \rightarrow \gamma^* Y}(q_a^2, q^2, M_{\gamma^*}^2)|^2, \tag{11}$$

1921

where a factor $\alpha/(3\pi M^2)$ arises from integrating over the lepton pair angular distribution. In (9) $n_{ab \to cd}$ and $n_{a \to cd}$ denote the corresponding number of parton interactions that occur at given $\hat{s}$ and space-time point r. These are obtained from the explicit parton cascade simulation of an ensemble of nuclear collision events. The matrix elements are standard and can be found, for instance, in Ref. [6]. The kinematic variables $\hat{s}$, $\hat{t}$, and $\hat{u}$ refer to a pair of colliding partons ab, and q_a^2 is the invariant mass of a virtual parton a. The squared amplitudes for the processes (2)–(4) and for the pure QCD processes $ab \to cd$ and $a \to bc$ are evaluated with the standard running strong coupling $\alpha_s(M^2)$, where we take $M^2 = p_\perp^2$, except for $q\bar{q}$ annihilation, for which $M^2 = \hat{s}$, and for gluon bremsstrahlung, where $M^2 \simeq q_a^2$. Furthermore, a K factor is employed to account for higher order corrections to the lowest order cross sections in (10). This is implemented by adopting the prescription of [7] to replace $\alpha_s(M^2)$ in the cross sections by $\alpha_s(0.075\,M^2)$. The integration over $\hat{t}$ in (10) is limited by $\hat{t}_{min, max}(p_{\perp cut})$, where $p_{\perp cut}$ has been fixed from pp and $p\bar{p}$ scattering data [8] and its value for $\sqrt{s} = 200A$ GeV is $p_{\perp cut} = 1.5$ GeV. The upper limit of the q_a^2 integration of the widths Γ in (11) is given by the virtuality of parton a, $q_{max} = q_a$, and the lower limit is constrained by the minimum allowed parton virtuality $q_{min} = 1$ GeV, which has been determined for the parton cascade model in [5] from e^+e^- annihilation data.

Thus, according to (9), by summing over the complete space-time history of the partons' evolution in phase space up to a certain time τ, we can obtain the yield of dileptons from the various processes (1)–(5) as a function of time and observe how the total lepton pair production develops from the first nuclear contact via preequilibrium towards thermalization of the parton system.

In Fig. 2 we show $dN(\tau)/dM^2$, the invariant mass distribution of dilepton pairs with mass M^2, integrated over space-time up to different times τ during central Au+Au collisions at $\sqrt{s} = 200A$ GeV. Here the proper time τ is defined as $\tau = \text{sign}(t - t_0) \sqrt{(t - t_0)^2 - z^2}$, where t is the center-of-mass time and t_0 ($\simeq 1$ fm/c for $\sqrt{s} = 200A$ GeV) is the moment of maximum overlap of the colliding nuclei. Thus, in the center of mass, at $z = 0$ fm, the initial nuclear contact occurs at $\tau = -1$ fm/c and the maximum density is achieved at $\tau = 0$. It is obvious from the steepening of the distribution with time [curves (1)–(3)] that the high-mass pairs are mostly produced at early times. During later times pair production is essentially concentrated in the low-mass region $M \leq 3$ GeV. Note that the bending over of the distributions at lower masses is related to the aforementioned cutoffs used in the calculations, $p_{\perp cut} = 1.5$ GeV and $q_{min} = 1$ GeV. Therefore we do not think that our results are reliable below about 2 GeV. In this lower-mass region contributions from hadrons in the final state (not included here) are expected to be large anyway.

Figure 3 depicts the contributions from the various processes (1)–(5) to the integrated dilepton yield per unit rapidity at $y = 0$, dN/dM^2dy, integrated up to $\tau = 2$ fm/c. For $M \geq 4$ GeV the annihilation process $q\bar{q} \to l^+l^-$ dominates, but the process $gq(\bar{q}) \to l^+l^- q(\bar{q})$ also contributes considerably because of the much larger number of $gq(\bar{q})$ collisions. The low-mass pairs with $M \leq 2$ GeV are mainly from the bremsstrahlung processes $q(\bar{q}) \to l^+l^- q(\bar{q})$. The process $q\bar{q} \to l^+l^- g$ contributes about an order of magnitude less than the direct

Time evolution of l^+l^--production

Au+Au (b=0), $s^{1/2}$ = 200 A GeV

(1) $\tau \leq$ -0.4 fm/c
(2) $\tau \leq$ -0.1 fm/c
(3) $\tau \leq$ 0.5 fm/c
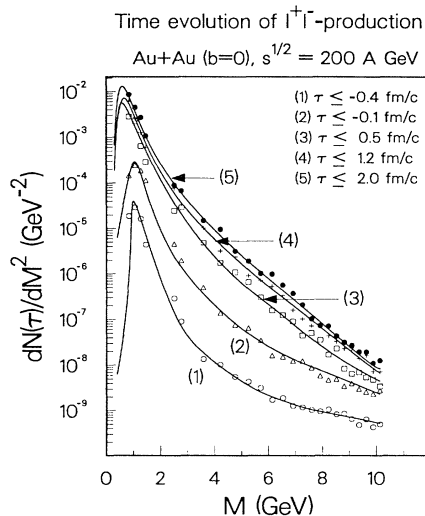(4) $\tau \leq$ 1.2 fm/c
(5) $\tau \leq$ 2.0 fm/c

FIG. 2. Time development of the invariant mass distribution of l^+l^- pairs during central Au+Au collisions at $\sqrt{s} = 200A$ GeV. The time $\tau = 0$ corresponds to the moment of maximum nuclear overlap. The data points result from the parton cascade simulation; the lines are interpolations to guide the eye.

Contributions to l^+l^--production

Au+Au (b=0), $s^{1/2}$ = 200 A GeV

$\square$ $q\bar{q}$ -> γ -> l^+l^-
$\times$ gq -> γq -> l^+l^- q
$\triangle$ $q\bar{q}$ -> γg -> l^+l^- g
$\circ$ gg -> γg -> l^+l^- g
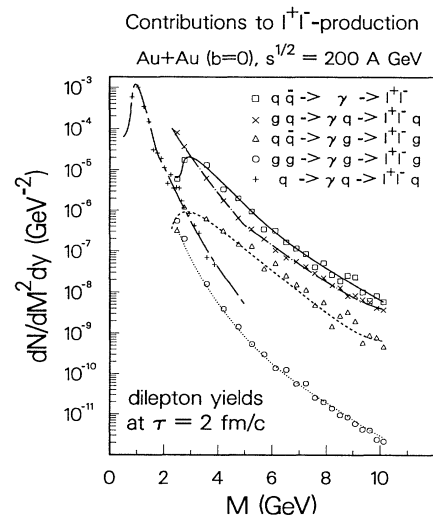$+$ q -> γq -> l^+l^- q

dilepton yields
at $\tau = 2$ fm/c

FIG. 3. Individual contributions from the dilepton production processes (1)–(5) to the space-time integrated distribution $dN/dM^2dy|_{y=0}$ after $\tau = 2$ fm/c in central Au+Au collisions at $\sqrt{s} = 200A$ GeV.

annihilation $q\bar{q} \to l^+l^-$ and the process $gg \to l^+l^- g$ is suppressed by 3–4 orders and is therefore negligible.

Finally, Fig. 4 shows the total dilepton distribution dN/dM^2dy at $y = 0$ integrated over space-time up to $\tau = 2$ fm/c, as well as the three separate contributions from parton interactions involving exclusively primary partons ("Drell-Yan"), primary plus secondary partons, and only secondary partons. Here "primary" refers to those, in some sense preexisting, partons pulled from the structure functions, whereas "secondary" partons are those that have scattered at least once or have been created during the collision. Also shown are the dilepton yields from a quark-gluon plasma that one gets from the process (1) within hydrodynamical and free-streaming evolution scenarios [9], from an initial time $\tau_0 = 2$ fm/c and temperature $T_0 \equiv T(\tau_0) = 300$ MeV, corresponding to the actual conditions at the end of the computer simulation [4], to a phase transition at a temperature $T_c = 180$ MeV. These are estimates of the contribution to the dilepton yield at later times. It is remarkable how smoothly the total distribution of the parton cascade simulation for $\tau \leq 2$ fm/c merges into the dilepton distributions corresponding to a quark-gluon plasma evolution from $\tau > \tau_0 = 2$ fm/c. Most notable, however, is the overwhelming production of dileptons from the primary-secondary and secondary-secondary interactions relative to the "Drell-Yan" processes (primary-primary interactions). For masses greater than 2 (4) GeV we would expect about 20 (1) lepton pairs per hour at RHIC, as-

suming a luminosity of 10^{26} cm^{-2}s^{-1} and triggering on impact parameters less than 2 fm. It is important to mention that almost all pairs are produced with rapidities $|y| \leq 4$, and that about 70% have $|y| \leq 1$. In order to achieve good statistics, the experiments must therefore concentrate on the central rapidity region, since the count rates from the beam fragmentation region are very small.

In conclusion, our computation of the lepton pair yield in central Au+Au collisions at RHIC with the parton cascade model results in a smooth evolution of the l^+l^- mass distribution from Drell-Yan towards quark-gluon plasma, with a clear dominance of pairs from preequilibrium and quark-gluon plasma over the Drell-Yan yield. Experiments in the central rapidity region are eagerly awaited to test our understanding of the many-body dynamics of quarks and gluons.

Note added.—Recently the dissipative mechanisms that precede the formation of a thermalized parton plasma have attracted considerable interest in the context of how preequilibrium dynamics affects the yield of dileptons [10]. The common conclusion of these studies is—in qualitative agreement with our prediction—that the yield of lepton pairs from the mass region around $m_{J/\psi}$ is significantly larger than the Drell-Yan background.

Contributions of interaction types
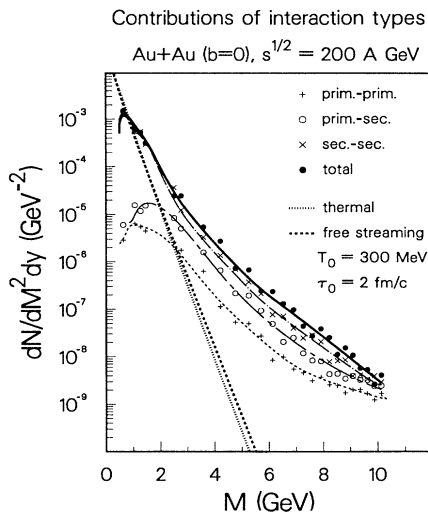
Au+Au (b=0), $s^{1/2} = 200$ A GeV

FIG. 4. Invariant mass distributions of dileptons in the central rapidity region in Au+Au collisions at $\sqrt{s} = 200A$ GeV. The bold solid line is the total l^+l^- yield from the parton cascade evolution after $\tau = 2$ fm/c. The three curves below show the separate contributions from "Drell-Yan" processes (primary-primary), from interactions involving primary with secondary partons, and from interactions involving only primary partons. The two steep straight lines correspond to the contributions from a quark-gluon plasma within hydrodynamical and free-streaming scenarios.

[1] E. V. Shuryak, Phys. Lett. **78B**, 150 (1978); K. Kajantie and H. I. Miettinen, Z. Phys. C **9**, 341 (1981); G. Domokos and J. Goldman, Phys. Rev. D **23**, 203 (1981).

[2] R. Hwa and K. Kajantie, Phys. Rev. D **32**, 1109 (1985); K. Kajantie, J. Kapusta, L. McLerran, and A. Mekjian, Phys. Rev. D **34**, 2746 (1986); K. Kajantie, M. Kataja, L. McLerran, and V. Ruuskanen, Phys. Rev. D **34**, 811 (1986).

[3] K. Geiger and B. Müller, Nucl. Phys. **B369**, 600 (1992).

[4] K. Geiger, Phys. Rev. D **46**, 4965 (1992); **46**, 4986 (1992).

[5] K. Geiger, Phys. Rev. D **47**, 133 (1993).

[6] R. D. Field, *Applications of Perturbative QCD*, Frontiers in Physics Vol. 77 (Addison-Wesley, Redwood City, CA, 1989).

[7] R. K. Ellis and J. C. Sexton, Nucl. Phys. **B269**, 445 (1986).

[8] N. Abou-El-Naga, K. Geiger, and B. Müller, J. Phys. G **18**, 797 (1992).

[9] J. Kapusta, L. McLerran, and D. K. Srivastava, Phys. Lett. B **283**, 145 (1992).

[10] B. Kämpfer and O. P. Pavlenko, Phys. Lett. B **289**, 127 (1992); I. Kawrakow and J. Ranft, Report No. UL-HEP-92-08, Leipzig, Germany (to be published); E. Shuryak and L. Xiong, Phys. Rev. Lett. (to be published).